Non-Linear Nanoscale Piezoresponse of Single ZnO Nanowires affected by Piezotronic effect

Helena Lozano[†‡‖] *Gustau Catalán* [§∓], *Jaume Esteve*[†], *Neus Domingo* [§‡*], *Gonzalo Murillo*[†‡*]

[†] Instituto de Microelectrónica de Barcelona, Bellaterra, 08193, Spain

[§] Catalan Institute of Nanoscience and Nanotechnology (ICN2), CSIC and The Barcelona Institute of Science and Technology, Campus UAB, Bellaterra, 08193 Barcelona, Spain

[∓] ICREA – Institució Catalana de Recerca i Estudis Avançats, 08010 Barcelona, Spain

[*]e-mail: neus.domingo@icn2.cat; gonzalo.murillo@csic.es;

[‡]These authors contributed equally

KEYWORDS: ZnO, Nanowire, PFM, piezotronics, C-AFM, piezoelectric coefficient, PENG, nanogenerator, piezoresponse.

Abstract

ZnO nanowires (NW) as semiconductor piezoelectric nanostructures have emerged as the focus material for applications in energy harvesting, photonics, sensing, biomedical science, actuators or spintronics. The expression of the piezoelectric properties in semiconductor materials is concealed by the screening effect of the available carriers and the piezotronic effect, leading to complex nanoscale piezoresponse signals. Here, we have developed a metal-semiconductor-metal model to simulate the piezoresponse of single ZnO nanowires, demonstrating that the apparent non-linearity in the piezoelectric coefficient arises from the asymmetry created by the forward and reversed biased Schottky barriers at the semiconductor–metal junctions. By directly measuring the experimental I-V characteristics of ZnO NWs with C-AFM together with the piezoelectric vertical coefficient by PFM, and comparing them with the numerical calculations for our model, effective piezoelectric coefficients in the range $d_{33\text{eff}}$ ~ 8.6 pm/V – 12.3 pm/V have been extracted for ZnO NWs. We have further demonstrated via simulations the dependence

between the effective piezoelectric coefficient d_{33eff} and the geometry and dimensions of the NW (radius to length ratio), revealing that the higher d_{33eff} is obtained for thin and long NW due to the tensor nature proportionality between electric fields and deformation in NW geometries. Moreover, the non-linearity of the piezoresponse also leads to multiharmonic electromechanical response observed at the second and higher harmonics that indeed is not restricted to piezoelectric semiconductor materials but can be generalized to any type of asymmetric voltage drops on a piezoelectric structure as well as leaky wide band-gap semiconductor ferroelectrics.

1. Introduction

Scavenging of ambient mechanical energy for its posterior utilization is becoming a hot research topic (Harb, 2011). Energy harvesting relies on a transduction force that converts the ambient mechanical energy into electricity. This mechanical energy can have different forms such as vibrations, random motions, noise, etc. The most common transduction methods are: electrostatic, electromagnetic, triboelectric and piezoelectric. A piezoelectric material has the peculiarity of creating an inherent electric field when strained (direct piezoelectric effect). Some examples of well-known piezoelectric materials are AlN, PZT, ZnO or quartz. Among those, ZnO has a non-central symmetric wurtzite crystal structure and a hexagonal unit cell. This structure has polar surfaces that can be described as a number of alternating planes composed of tetrahedrally coordinated O^{2-} and Zn^{2+} ions, stacked alternatively along the c-axis as is shown in Fig.S1. The oppositely charged ions produce positively charged (0001)-Zn and negatively charged (0001)-O polar surfaces, resulting in a normal dipole moment and spontaneous polarization along the c-axis as well as a divergence in surface energy. ZnO has become very popular in material science over the last few years because of its wide variety of nanostructures and its dual property of being both a semiconductor and piezoelectric material(Özgür *et al.*, 2005; Janotti and Van De Walle, 2009): it has a wide band gap (~3.37 eV), large exciton binding energy (~60 mV), it is relatively biosafe and biocompatible(Stitz *et al.*, 2016) and it exhibits an abundant configuration of nanostructures as nanowires (NWs)(Espinosa, Bernal and Minary-Jolandan, 2012), nanobelts, nanosheets or nanorings(Wang, 2009). Thanks to these properties, this material has numerous potential applications in energy harvesting, photonics, sensing, biomedical science, actuators, spintronics and optoelectronics(Yang *et al.*, 2002, 2012; Özgür *et al.*, 2005; Wang *et al.*, 2010; Wang, 2012; Murillo, Blanquer, *et al.*, 2017; Kang *et al.*, 2019). One of the most useful nanostructures that can be utilized to generate energy is the nanowire (NW)(Xu *et al.*, 2010; Espinosa, Bernal and Minary-Jolandan, 2012). These nanostructures are commonly referred to as nanogenerators, which have the advantage of being more flexible and less sensitive to fracture than generators based on thin-films. It was already demonstrated that a single ZnO NW can generate a

piezoelectric potential along it when strained. The generated energy output by one NW in one discharge event is about 0.05 fJ, and the output voltage on the load is around 8 mV, for a 5 nN force applied by an AFM tip (Wang and Song, 2006; Riaz *et al.*, 2011).

One of the main hindrances in the expression of the piezoelectric properties in semiconductor materials is the screening effect of the available carriers, concealing any piezoelectric voltage(Morozovska *et al.*, 2007). The entanglement between conductivity and piezoelectricity conceals the determination of net piezoelectric coefficients as measured by electromechanical sensing techniques such as Piezoresponse Force Microscopy (PFM), which on the other hand, is an ideal tool since it is able to measure this piezoelectric coefficient in one single nanostructure. In this work, we have developed a general model to describe nanoscale piezoresponse in piezoelectric semiconductors that deconvolutes the experimental effective piezoelectric response from the semiconductor screening effect. Moreover, we show how this entanglement leads to experimental non-linear piezoresponse signals and we demonstrate the emergence of multifrequency nanoscale electromechanical responses in the presence of Schottky barriers.

Due to the dual nature of ZnO, acting as semiconductor and piezoelectric material, in 2007, prof. ZL Wang introduced the fundamental principle of piezotronics (Zhong and Wang, 2007; Wang, 2010, 2012). Piezotronic effect is based on the influence of the piezoelectric potential with the electronic bands in the semiconductor, creating electronic components that can be triggered with strain. Also, the opposite effect can be found, where an external voltage applied to the material can affect its electronic bands and therefore affecting the generated strain due to the piezoelectric effect. Here, the dual properties of a ZnO nanostructure directly affect the piezoresponse at the nanoscale measured by PFM, and have to be taken into account.

2. Methods

ZnO can be grown by different bottom-up approaches such as vapor-liquid-solid, chemical vapor deposition or hydrothermal method. However, a crystalline substrate with a similar lattice constant is the best choice in order to obtain aligned and high-quality NWs (Vayssieres, 2003; Jin

et al., 2005; Kwon *et al.*, 2012). Here, we use a hydrothermal method which is one of the most powerful low-cost, low-temperature and simple approaches to grow c-axis-aligned NWs. This method is based on an aqueous solution chemical reaction at low temperature (< 80 °C) directly on the silicon substrate covered by a seed layer (Murillo, Rodríguez-Ruiz and Esteve, 2016; Murillo, Lozano, *et al.*, 2017). The height and diameter of the NWs is determined by the growth time, temperature and concentration. For the ZnO NW growth, a silicon wafer with a seed layer of evaporated gold with a chromium adhesion layer (50 nm Au/ 20 nm Cr) is commonly used to favor the nucleation. Every chip is then placed floating downward inside a wide-mouth jar containing the aqueous solution consisting of zinc nitrate hexahydrate ($Zn(NO_3)^{2-}$hexahydrate) and hexamethylenetetramine (HMTA) [1:1] 5 mM each purchased from Sigma-Aldrich. Subsequently, the pot is closed and introduced in an oven at 70°C for 16h. A scheme of this process is shown in Fig.S2 and a more detailed description is presented in the Supplementary information. Fig.1 shows SEM and AFM images of the ZnO NWs. As can be seen, the gold activation method ensures a well orientation and distribution of ZnO NW growth. The average height of the obtained NW is $h = 1.2 \pm 0.2$ µm and the average radius is $r = 0.9 \pm 0.15$ µm (Murillo, Lozano, *et al.*, 2017).

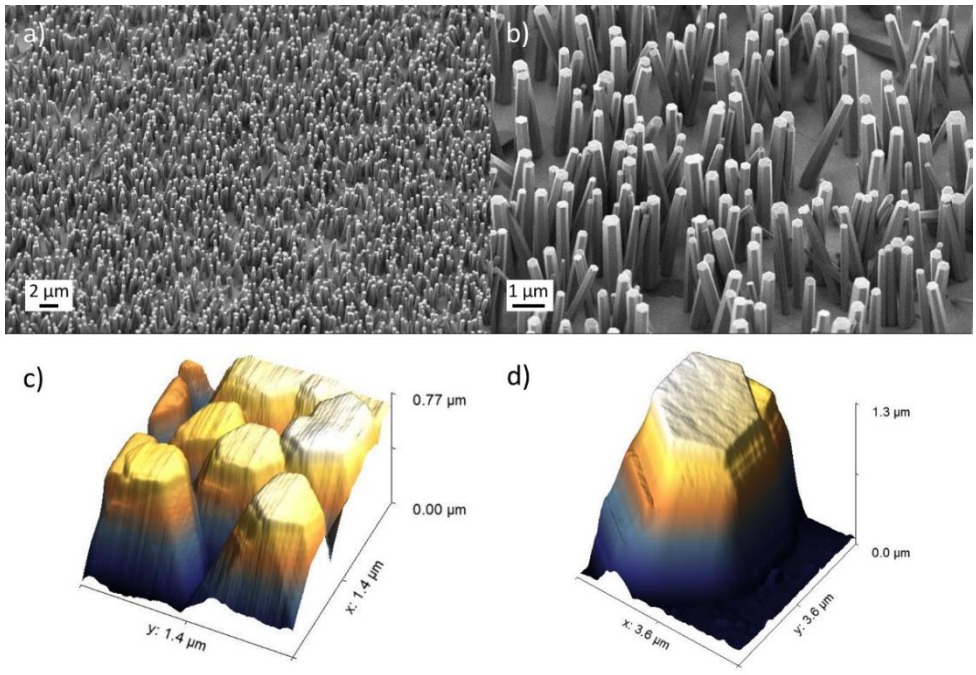

Fig.1: a) and b) SEM image of the ZnO NWs. c) AFM 3D topography image of several ZnO NWs and d) one single NW.

Piezoresponse Force Microscopy (PFM) depicted in a scheme in Fig.2a has become a standard for imaging ferroelectric domain patterns or for studying the piezoelectricity of certain materials (Kalinin, Karapetian and Kachanov, 2004). PFM is an extension of contact mode AFM technique and it is based on the converse piezoelectric effect of the material under test. A conductive AFM probe tip is used as a top electrode to simultaneously measure the mechanical response when an electrical voltage is being applied to the sample surface. Then, in response to the electrical stimulus, the sample locally expands or contracts linearly according to the material piezoelectric coefficient. Usually an *ac* voltage (V_{ac}) is used to excite the sample, because it allows the use of a lock-in amplifier to read-out the tiny motion generated by the converse piezoelectric effect. In this case, if V_{ac} is the voltage applied by the tip and d_{33} is the piezoelectric coefficient in the z-axes, the amplitude of the vibration as measured by an AFM tip in the vertical direction is described by eq. 1:

$$A_{PFM} = d_{33}V_{ac} \qquad (1)$$

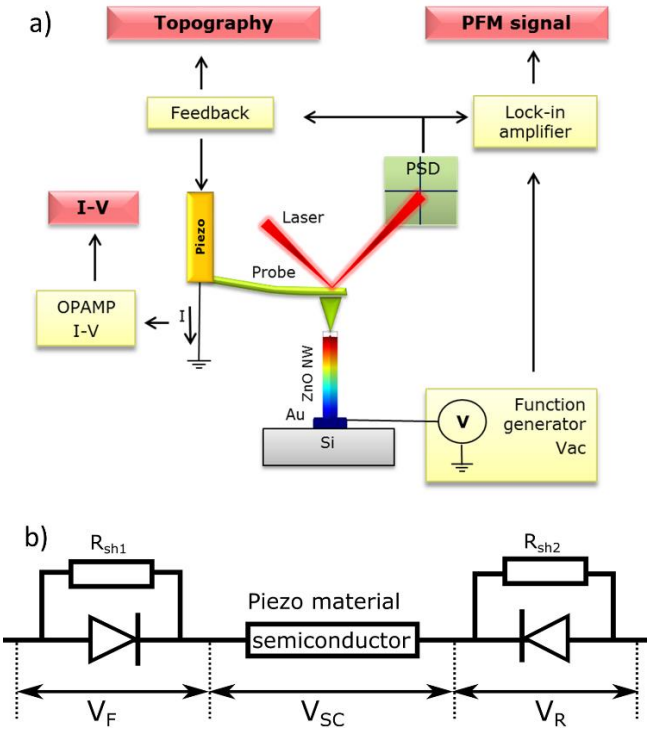

Fig.2: a) Scheme of the PFM setup. b) Schematic diagram of the equivalent circuit of the Pt/ZnO/Au corresponding to a M-S-M structure, where R_{sh1} and R_{sh2} are the shunt resistors associated with both Schottky contacts. V_F is the voltage drop across the forward-biased Schottky barrier, V_R is the voltage drop across the reversed-biased Schottky barrier and V_{SC} is the voltage on the semiconductor, this is, the ZnO NW.

3. Results and discussion

Following this relationship, it is possible to determine the effective $d_{33\text{eff}}$ coefficient of a piezoelectric dielectric material by measuring the linear change in PFM amplitude as a function of the applied *Vac* voltage magnitude. Most of the materials that exhibit piezoelectricity are insulators for which the applied voltage between the AFM probe tip and sample substrate is fixed and well-known, but still quantification of piezoelectric coefficients by PFM is a controversial issue due to several factors such as i) the real distribution of electric field through the sample, ii) undesired crosstalk between the tip and the sample due to electrostatic coupling, iii) instrumental artifacts and iv) possible flexoelectric effects due to the presence of strain and electric field gradients around the AFM tip (Abdollahi, et al., 2019). However, piezoelectricity can also be found in semiconductor crystals with non-central symmetry, especially those who have a wurtzite structure such as ZnO. One of the major issues when measuring piezoelectricity in semiconductors is that for an adequate charge separation generated by piezoelectricity during an applied stress, free carriers must not be allowed to travel through the semiconductor (in our case ZnO NW), otherwise the generated electric field across the semiconductor will be partly neutralized. On another hand, semiconductors under a voltage drop can indeed carry a current depending on the doping and the electrical connections or junctions. For the case of piezoelectric semiconductors, when a voltage is applied, current can flow through the NW reducing the effective electric field inside the nanostructure. Electronic characteristics of semiconductor materials such as *I-V* curves can be measured by Conductive AFM (C-AFM) thanks to the operational amplifier (OPAMP) located in the tip holder that is used to measure the small currents passing through the tip-sample contact area (see Supporting Information for experimental

details)(Wen *et al.*, 2019). In this sense, the simultaneous determination of the current profile as a function of the applied voltage will allow us to stablish the effective voltage drop at the semiconductor that will promote the net effective electromechanical response.

The current-voltage (*I-V*) characteristic of a semiconducting device depends on a range of parameters of the semiconductor material, such as its resistivity, doping concentration and carrier mobility, but in our case we will specially focus on the dependence of the geometry and the properties of its contacts. From the electronic point of view, our system is composed by a gold seed layer, a ZnO NW and a tip with a Pt coating (Fig. 2a) and can be described as a Metal-Semiconductor-Metal (M-S-M) structure(Elhadidy, Sikula and Franc, 2012). This fact is essential to understand the piezoresponse signals in semiconductor piezoelectrics since an M-S-M structure will show different *I-V* characteristics as a function of the type of metal-semiconductor contacts: while Ohmic contacts lead to linear characteristics, the inclusion of a Schottky contact will lead to a rectifying *I-V* curve(Panda; *et al.*, 2013; Lee *et al.*, 2016; Lord *et al.*, 2017). In this case, as shown in Fig. 2b we have modeled the ZnO NW embedded between two electrodes as two Schottky barriers head-to-head in series with a resistor (R_{SC}) that originates from the undepleted part of the semiconductor. When one applies a bias voltage to this structure, one of the Schottky contacts is forward biased and the other one is reverse biased, and thus the total *I-V* characteristic is neither linear nor rectifying, but instead it becomes almost symmetric due to the resulting electric field dependence of the barrier height(Elhadidy, Sikula and Franc, 2012). The current-voltage relationships of the three series are: i) forward-biased Schottky barrier ($I_F - V_F$), ii) semiconductor/piezo material ($I_{SC} - V_{SC}$) and iii) reverse-biased Schottky barrier ($I_R - V_R$) ("image force" effect) leading to a full voltage drop $V = V_F + V_R + V_{SC}$ (Elhadidy, Sikula and Franc, 2012). In the framework of the thermionic emission theory, the $I_F - V_F$ curve at the forward-biased Schottky junction is given by eq. 2: according to the:

$$I_F = I_{01}\left[\exp\left(\frac{qV_F}{kT}\right) - 1\right] + \frac{V_F}{R_{sh1}} \qquad (2)$$

where

$$I_{01} = A_1 A^* T^2 \exp\left(-\frac{q\phi_{b1}}{kT}\right) \quad (3)$$

In this case, ϕ_{b1} is the barrier height at the zero bias, $A^* = 4\pi e m^* k^2/h^3$ is the Richardson constant, *k* is the Boltzmann constant, *T* is the absolute temperature, m^* is the hole effective mass, *h* is Planck's constant, *q* is the magnitude of the electronic charge and A_1 is the contact area. On the other hand, the reverse current density of the Schottky diode results on:

$$I_R = I_{02}\left[\exp\left(\frac{q\Delta\phi_b}{kT}\right) - 1\right] + \frac{V_R}{R_{sh2}} \quad (4)$$

Where

$$I_{01} = A_2 A^* T^2 \exp\left(-\frac{q\phi_{b2}}{kT}\right) \quad (5)$$

where, ϕ_{b2} is the barrier height and A_2 is the contact area for the reverse-biased Schottky barrier and $\Delta\phi_b$ is the barrier lowering due to the maximum electric field strength, E_0. The Schottky effect barrier lowering due to the image force is given by:

$$e\Delta\phi_b = \sqrt{\frac{qE_0}{4\pi\varepsilon_S}} \quad (6)$$

and

$$E_0 = \sqrt{\frac{2qN_A(V_R + V_{i2} - kT/q)}{\varepsilon_S}} \quad (7)$$

where N_A is the carrier density in the semiconductor and ε is the semiconductor permittivity. The reverse current of ideal Schottky contacts should saturate at a very low value, independent of the applied voltage. However, there are several causes of deviation from this ideal behavior: tunneling through the barrier becomes the dominating component under the reverse bias in low-dimensional systems while for semiconductor devices with a low carrier concentration working at room temperature, the lack of saturation of the reverse current could be also explained by the barrier lowering at the M-S interface. It is to mention that the nature of the Schottky barrier in ZnO structures has also a relevant effect on the piezotronic applications of this material(Keil *et al.*, 2017; Li *et al.*, 2017).

Finally, assuming that the undepleted part of the semiconductor is homogeneous and has a constant resistance, R_{SC}, the $I_{SC} - V_{SC}$ relationship for the semiconductor is simply:

$$I_{SC} = \frac{V_{SC}}{R_{SC}} \tag{8}$$

and since the current flowing through each part of the M-S-M structure is the same as for a steady current(Elhadidy, Sikula and Franc, 2012), we have:

$$I = I_R = I_F = I_{SC} \tag{9}$$

Fig.3a shows the characteristic I-V curve of a single ZnO NW as measured by C-AFM using a Pt-coated tip as a mobile top electrode. Since in our configuration the voltage is applied to the sample, the *I-V* characteristics at the positive voltages corresponds to the Pt-ZnO junction, while at the negative voltages is assigned to the Au-ZnO junction. Computer simulations, using a written Matlab code, based on the M-S-M model were performed to calculate the real voltage drop at the semiconductor ZnO NW structure. First, the experimental *I-V* curve is simulated considering the M-S-M structure and equations (2-9). The parameters used in the simulations were initially taken from the literature and adjusted to our model based on the right fitting to the experimental *I-V* curves, and are listed in Table 1. Fig.3a shows the simulated pseudo symmetrical total *I-V* curve resulting from our structure overimposed to the experimental measurement. The obtained asymmetry is due to the difference in the work function of the platinum ($\Phi_{Pt} = 5.6\ eV$) and gold ($\Phi_{Au} = 5.8\ eV$), non-identical area of contacts (the ZnO NW - Au substrate contact area corresponds to the NW diameter while the ZnO NW - $PtIr_5$ tip contact area is smaller than the tip radius), shunt resistances, pinning of the Fermi energy levels by the surface states and the existence of the interfacial insulating layers at both electrode contacts. Notice that the simulation curves are in well agreement with the experimental measurements.

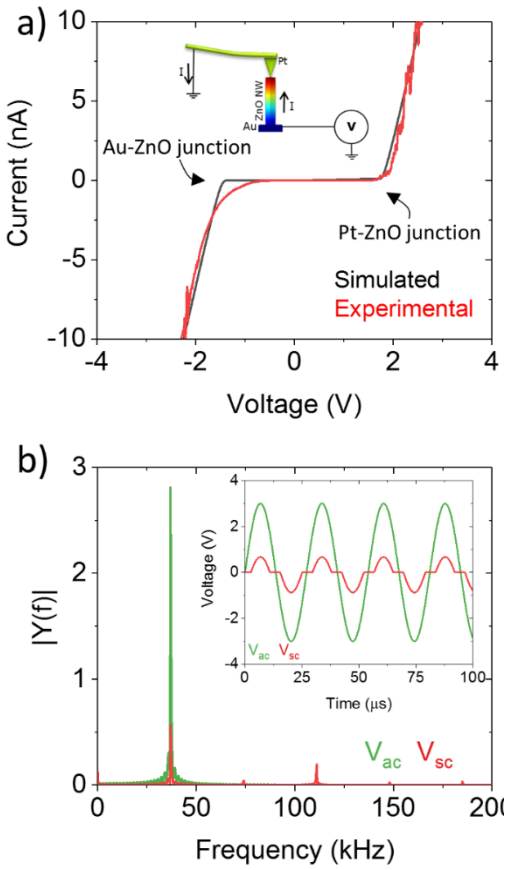

Fig.3: a) *I-V* curve of a single ZnO NW as measured by C-AFM (red line) and simulated I-V curve for a M-S-M structure (black line) as explained in the text using parameters shown in Table 1. The breaking point is not the same due to the difference between the Au-ZnO junction and the Pt-ZnO junction, producing the asymmetry in the *I-V* curve. The inset shows the scheme of the C-AFM set up, where the voltage is applied to the bottom electrode. b) Transfer function of two different symmetric and asymmetric functions (shown in the inset) into the frequency space, showing their contribution to different harmonics. For an ideal sinusoidal function as that used as an excitation bias V_{ac} there is only a contribution in the first harmonic (green line). Instead, for an asymmetric excitation voltage as that calculated for the semiconductor voltage drop V_{SC} using eq. 2-9 (potential difference along the ZnO NW), there is a relevant contribution to multiple higher harmonics (green line).

Table 1: List of parameters used in the simulations for the voltage drop at the semiconductor.

Parameter	Symbol	Value
Work function of the platinum	Φ_{Pt}	5.65 eV
Work function of the gold	Φ_{Au}	5.8 eV
Electron affinity of ZnO	χ_{ZnO}	3.7 eV
ZnO NW resistivity	R_{ZnO}	60 MΩ
Electrical permittivity of ZnO	ε_{ZnO}	5.7
Diffusion potential at the contact	V_{i2}	0.4 V

Assuming an ideal sinusoidal function for the V_{ac} voltage applied to the tip (green line in Fig.3b inset), and considering the *I*-*V* characteristics measured by C-AFM (as shown in Fig.3a), the resulting simulated voltage along the piezo V_{SC} is presented in Fig.3b (inset, red line). As can be seen, the effective voltage drop in the NW is no longer symmetric but shows a threshold value together with a strong asymmetry. This fact is very relevant to the interpretation of the piezoresponse signal since i) this will lead to non-linear piezoresponse as a function of the applied voltage and ii) it will originate electromechanical responses at the higher harmonics of the excitation frequency leading to multiharmonic PFM response. As opposite to an ideal piezoelectric response under a symmetric applied voltage, where the electromechanical signal is only in the first harmonic, the frequency response of the signal shown in Fig.3b will also show contributions into higher harmonics of the signal. Beyond the present case for a M-S-M structure, the multifrequency piezoresponse is indeed a general phenomenon that can be found in any piezoelectric material arising from the application of asymmetric excitation voltages e.g., due to the use of non-equivalent electrodes.

In addition, the effective electromechanical signal in the first harmonic will be reduced by this effect. Due to the asymmetrical *I*-*V* curve and the modulated voltage applied in the NW, the real voltage drop at the NW is not linear. In order to calculate the voltage distribution along the M-S-M structure (V_F, V_R and V_{SC} from Fig.2b) and their variation with the applied voltage, the equations (2 – 9) are numerically solved. The results are shown in Fig. 4a, taking the parameters presented in table 1. Fig. 4a shows that, as the excitation *ac* bias voltage magnitude (V_{ac}) increases,

the voltage drop across the reversed-biased Schottky barrier (V_R) increases rapidly and becomes dominating until the voltage on the semiconductor bulk (V_{SC}) becomes notable. At the same time, the voltage drop across the forward-biased Schottky barrier (V_F), remains negligible. It is clear that the range in which the voltage drop across the reverse-biased Schottky barrier (V_R) is dominant depends on the value of the resistance of the semiconductor, in this case, the ZnO NW (R_{ZnONW}). V_R increases and decreases as R_{ZnONW} decreases and increases, respectively. At a large bias and in the case of a high value of R_{ZnONW} the voltage V_R starts to saturate, while the voltage V_{SC} across the semiconductor bulk increases almost linearly. Also, V_F starts to increase slowly. In this large bias regime, the change of the voltage across the semiconductor bulk is responsible for the change of the bias.

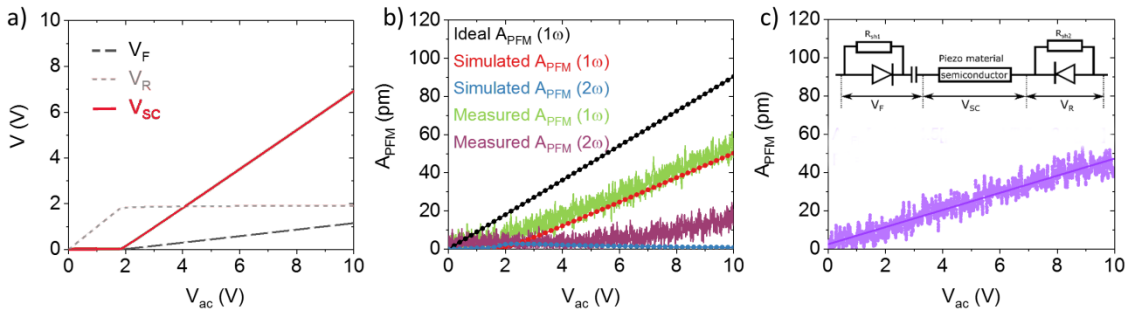

Fig.4: a) Simulated voltage amplitudes along the different parts of the M-S-M structure as a function of the excitation bias amplitude V_{ac}: forward-biased Schotkky junction (V_R – grey dotted line), reversed-biased Schotkky junction (V_F – black dash line) and semiconductor ZnO NW (V_{SC} – red line). The voltage drop along the piezoelectric material V_{SC} is lower than the bias voltage V_{ac} due to the current that flows through the NW. b) PFM amplitude signal as a function of the excitation bias: the black line shows an ideal d_{33} curve with a slope corresponding to $d_{33\text{eff}} = 9.6$ pm/V. Measured piezoresponse signal A_{PFM} (1ω) plotted in green showing a non-linear behavior with apparent lower slope together with a relevant multifrequency response as shown by the PFM signal at the second harmonic (2ω), plotted in purple. From this measurement, the apparent effective piezoelectric coefficient $d_{33\text{eff}}$ would be lower than the theoretical d_{33}. However, the red line shows the simulated piezoresponse signal A_{PFM} (1ω) taking a piezoelectric coefficient of

d_{33eff} = 9.6 pm/V and assuming the M-S-M model, in full agreement with the experimental curve. c) PFM amplitude signal measured on a NW covered by an insulating layer of 5 nm of alumina. In this case, the sample shows a linear response and the corresponding fitting gives a value of d_{33eff} = 4.5 pm/V. The inset shows the new electronics configuration for the structure of Pt/Al_2O_3/ZnO/Au, which can be described as a capacitor included in series between the forward Schottky barrier and the semiconductor, breaking the M-S-M structure.

Because the generated piezoelectric displacement (A_{PFM}) is linearly related to the voltage applied to the piezoelectric material (V_{SC}) (eq. 1), a PFM signal with two differentiated regions should also be expected. The PFM amplitude is simulated using eq. 1 by substituting V_{ac} by V_{SC}. As can be seen from Fig.4b, the real PFM signal in the first harmonic has a non-linear behavior, as expected from the effective voltage drop V_{SC} at the semiconductor (Fig.4a). The linear part of the response has a lower slope as compared to the ideal signal obtained for a pure dielectric piezoelectric, leading to an apparent lower than real value. In addition, a measurable PFM signal appears in the second harmonic.

The multiharmonic response for the PFM amplitude as a function of V_{ac} measured for ZnO NW is presented in Fig.4b. The effective piezoelectric coefficient has been calculated by fitting the experimental data with the simulations giving a value of d_{33eff} = 9.6 ± 2.5 pm/V. The variability on the experimental results is attributed to the tip damage, alteration of the surface states that may modify surface charge and carriers(Yang *et al.*, 2019) or the changes in the contact area between the tip and the NW, and is in good agreement with previously reported results using similar techniques(Tamvakos *et al.*, 2015; Su, 2017; Fortunato *et al.*, 2018; Lim *et al.*, 2018). This d_{33eff} coefficient has been calculated by assuming a capacitor like structure in which the electric field can be taken as homogeneous. Still, this assumption is far from the real electric field lines around an AFM tip, which is closer to a radial distribution. In the limit case of considering an electric field distribution as that created by a punctual charge, the voltage drop along the sample would differ by a factor of 2 with respect to the nominal one (Sitz, 2016) (Kalinin and Bonnell, 2002),

leading to an effective piezoelectric coefficient that would double the one calculated here, that can be taken as a lower limit value.

Finally, in order to avoid the current flow through the NW thus cancelling the Schottky barrier effect, an insulator layer of 5 nm of alumina (Al_2O_3) was deposited over the NWs by Atomic Layer Deposition (ALD). The presence of the alumina layer changes the configuration of the system breaking the M-S-M structure by adding a capacitor that eliminates the behavior of the two Schottky confronted diodes. Fig.4c shows the electronic configuration for this system and the measured PFM amplitude response as a function of the V_{ac} for the ZnO NW under the alumina layer. In this case, the response recovers the linear behavior but the linear fitting gives a lower coefficient of d_{33eff} = 4.5 pm/V (lower slope), probably due to effect of the insulating layer.

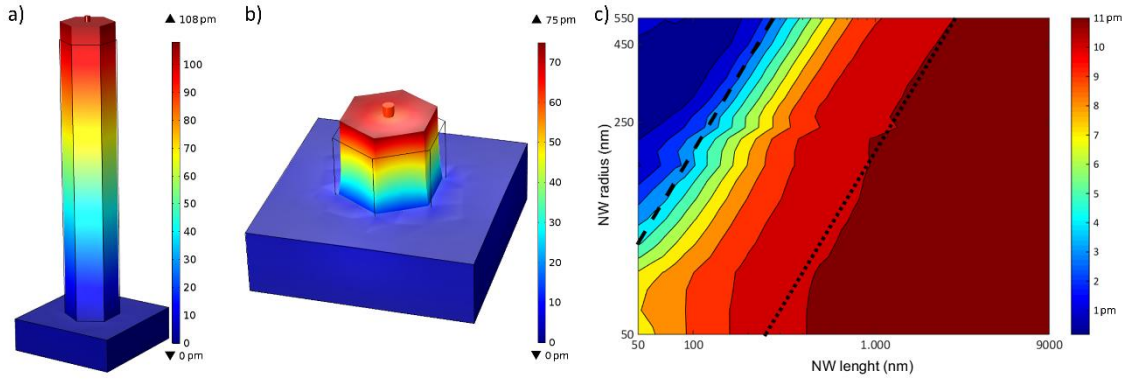

Fig.5: Total deformation of a single ZnO NW under an applied voltage of 10V due to the piezoelectric effect for a) a ZnO NW of 5 μm of height and 500 nm of radius and b) a ZnO NW of 600 nm of height and 500 nm of radius. c) 3D plot of the calculated effective piezoelectric coefficient d_{33eff} (color scale) as a function of the length (x-axis) and the radius (y-axis) of a ZnO NW. The calculation shows that for thick and short NW the d_{33eff} is lower than for thin and long NW.

To conclude, we have analyzed the dependence between the effective piezoelectric coefficient d_{33eff} and the geometry(Kim *et al.*, 2012) and dimensions of the NW using the piezoelectric module of COMSOL Multiphysics to simulate the piezoelectric response for different ZnO NWs

dimensions. The geometry of the simulated model is an hexagonal column of 500 nm of radius and 5 μm and 600 nm of height that represents the ZnO NW shown in Fig. 5a and Fig. 5b respectively. The Au substrate is designed as a block of 2 μm x 2 μm x 0.6 μm at the bottom of the NW and at the top of the NW a cylinder of 100 nm of height and 50 nm of radius emulates the Pt tip. Following the experimental configuration, the Au block is defined as a terminal and the tip as ground in the COMSOL piezoelectric module. Fig.5a and Fig.5b show the total displacement of the NW due to the piezoelectric effect: after applying 10 V the NWs show a deformation of 108 pm and 75 pm respectively. Notice that the total displacement is higher for a long thin NW than for thick and short NW. To study the NW radius effect, we perform a sweep in the NWs dimensions. Fig.5c shows a 3D plot of the behavior of the effective piezoelectric coefficient as the length and the radius of the NW is changed and the color range shows the piezoelectric coefficient. For thick and short NW, the d_{33eff} is lower than for thin and long NW and the obtained piezoelectric coefficient values are in the range between 1 and 11 pm/V. The decrease of d_{33eff} for thicker geometries can be explained taking into account two different effects: i) the radial distribution of the electric field due to the small tip size as compared to the NW geometry is bigger for higher radius, increasing the divergence of the real electric field distribution from that of a parallel plate capacitor, leading to a lower effective d_{33} coefficient corresponding to a deformation in the NW axis direction; ii) for bigger radius, there is stronger lateral constrain that prevents vertical expansion of the samples around the point of application of the electrical field. Moreover, since the piezoelectric coefficient is itself a tensor, one can observe that the sample deformation, after the application of a fixed voltage, stays constant over a fixed radius to length ratio, evidencing the fact that the piezoelectric effect is indeed including the whole volume of the NW through the tensor proportionality between deformation and applied field. The obtained experimental results of d_{33eff} ~9 pm/V for ZnO NW of 1.2 μm of length and 900 nm of radius falls within the expected range.

4. Conclusion

In summary, in this work we have developed a full electromechanical response model for piezoelectric semiconductors with asymmetric electrodes based on an M-S-M piezotronic structure, also suitable for leaky ferroelectrics that behave as wide band-gap semiconductors. We have demonstrated that the apparent non-linearity in the piezoelectric coefficient is generated by i) the asymmetry created by the Schottky barrier at the semiconductor–metal junctions and ii) the effective voltage drop at the ZnO nanowire due to partial screening of the electric field by the semiconductor carriers. Moreover, this non-linearity leads also to multiharmonic electromechanical response generating a PFM signal at the second and higher harmonics. Multifrequency PFM response is indeed not restricted to piezoelectric semiconductor materials but is general phenomenon that can be found in any piezoelectric material arising from the application of asymmetric excitation voltages as those created by different top and bottom electrodes materials. By directly measuring the experimental I-V characteristics of ZnO NWs with C-AFM together with the piezoelectric vertical coefficient by PFM, and comparing them with simulations, effective piezoelectric coefficients in the range $d_{33\text{eff}} \sim 8.6$ pm/V – 12.3 pm/V have been extracted for ZnO NWs which perfectly match the simulations resulting from the proposed theoretical model. Finally, a useful computational tool to predict the piezoresponse of semiconducting nanowires measured by PFM has been generated, revealing the strong effect of tensor nature proportionality between electric fields and deformation in NW geometries, demonstrating the dependence of the piezoelectric coefficient with the radius to length ratio.

ASSOCIATED CONTENT:

Supporting Information:

Description of ZnO crystalline structure showing the atomic model of the wurtzite structure of ZnO and its associated piezopotential; synthesis method with the experimental setup for the

nanowire's growth together with a scheme of the NWs growth using the hydrothermal method; experimental details of the PFM and C-AFM measurements.

AUTHOR INFORMATION:

Corresponding Author

E-mail: neus.domingo@icn2.cat; gonzalo.murillo@csic.es;

Present Addresses

[‖] Institute for Bioengineering of Catalonia, Barcelona, 08028, Spain

Notes:

The authors declare no competing financial interest.

ACKNOWLEDGEMENTS:

Financial support was obtained under projects from the Spanish Ministerio de Economía y Competitividad (MINECO) under project FIS2015-73932-JIN, H2020 ECSEL-JU under EnSO project (Energy for Smart Objetcs) (Contract n. 692482) and La Caixa Foundation under the Junior Leader Retaining program. In addition, this work was partially funded by 2017-SGR-579 from the Generalitat de Catalunya. ICN2 is supported by the Severo Ochoa program from Spanish MINECO (Grant No. SEV-2017-0706).

REFERENCES:

Elhadidy, H., Sikula, J. and Franc, J. (2012) ‘Symmetrical current–voltage characteristic of a metal–semiconductor–metal structure of Schottky contacts and parameter retrieval of a CdTe structure’, *Semiconductor Science and Technology*, 27(1), p. 015006. doi: 10.1088/0268-1242/27/1/015006.

Espinosa, H. D., Bernal, R. A. and Minary-Jolandan, M. (2012) ‘A review of mechanical and electromechanical properties of piezoelectric nanowires’, *Advanced Materials*, 24(34), pp. 4656–4675. doi: 10.1002/adma.201104810.

Fortunato, M. *et al.* (2018) ‘Piezoelectric Thin Films of ZnO-Nanorods/Nanowalls Grown by Chemical Bath Deposition’, *IEEE Transactions on Nanotechnology*, 17(2), pp. 311–319. doi: 10.1109/TNANO.2018.2800406.

Harb, A. (2011) ‘Energy harvesting: State-of-the-art’, *Renewable Energy*. Elsevier Ltd, 36(10), pp. 2641–2654. doi: 10.1016/j.renene.2010.06.014.

Janotti, A. and Van De Walle, C. G. (2009) ‘Fundamentals of zinc oxide as a semiconductor’, *Reports on Progress in Physics*, 72(12). doi: 10.1088/0034-4885/72/12/126501.

Jin, C. *et al.* (2005) ‘Epitaxial growth of zinc oxide thin films on silicon’, *Materials Science and Engineering: B*, 117, pp. 348–354. doi: 10.1016/j.mseb.2004.12.003.

Kalinin, S. V., Karapetian, E. and Kachanov, M. (2004) ‘Nanoelectromechanics of piezoresponse force microscopy’, *Physical Review B - Condensed Matter and Materials Physics*, 70(18), pp. 1–24. doi: 10.1103/PhysRevB.70.184101.

Kalinin, S. V and Bonnell, D. A. (2002) ‘Imaging mechanism of piezoresponse force microscopy of ferroelectric surfaces’, *Physical Review B*. American Physical Society, 65(12), p. 125408.

Kang, Z. *et al.* (2019) 'Interface Engineering for Modulation of Charge Carrier Behavior in ZnO Photoelectrochemical Water Splitting', *Advanced Functional Materials*, 29(15), p. 1808032. doi: 10.1002/adfm.201808032.

Keil, P. *et al.* (2017) 'Piezotronic effect at Schottky barrier of a metal-ZnO single crystal interface', *Journal of Applied Physics*, 121(15), p. 155701. doi: 10.1063/1.4981243.

Kim, S. M. *et al.* (2012) 'Radially dependent effective piezoelectric coefficient and enhanced piezoelectric potential due to geometrical stress confinement in ZnO nanowires/nanotubes', *Applied Physics Letters*, 101(1), p. 13104. doi: 10.1063/1.4731779.

Kwon, B. J. *et al.* (2012) 'Synthesis of vertical arrays of ultra long ZnO nanowires on noncrystalline substrates', *Materials Science and Engineering B: Solid-State Materials for Advanced Technology*. Elsevier B.V., 177(2), pp. 132–139. doi: 10.1016/j.mseb.2011.10.020.

Lee, J. A. *et al.* (2016) 'Schottky nanocontact of one-dimensional semiconductor nanostructures probed by using conductive atomic force microscopy', *Nanotechnology*. IOP Publishing, 27(42), p. 425711. doi: 10.1088/0957-4484/27/42/425711.

Li, Y. *et al.* (2017) 'Analysis on the piezotronic effect in a strained piezo-Schottky junction with AC impedance spectroscopy', *Nano Energy*, 36, pp. 118–125. doi: https://doi.org/10.1016/j.nanoen.2017.04.021.

Lim, T. *et al.* (2018) 'Crystal growth and piezoelectric characterization of mechanically stable ZnO nanostructure arrays', *CrystEngComm*. The Royal Society of Chemistry, 20(38), pp. 5688–5694. doi: 10.1039/C8CE00799C.

Lord, A. M. *et al.* (2017) 'Stability of Schottky and Ohmic Au Nanocatalysts to ZnO Nanowires', *Nano Letters*. American Chemical Society, 17(11), pp. 6626–6636. doi: 10.1021/acs.nanolett.7b02561.

Morozovska, A. N. *et al.* (2007) 'Piezoresponse force spectroscopy of ferroelectric-

semiconductor materials', *Journal of Applied Physics*, 102(11), p. 114108. doi: 10.1063/1.2818370.

Murillo, G., Blanquer, A., *et al.* (2017) 'Electromechanical Nanogenerator-Cell Interaction Modulates Cell Activity', *Advanced Materials*, 29(24), p. 1605048. doi: 10.1002/adma.201605048.

Murillo, G., Lozano, H., *et al.* (2017) 'Improving Morphological Quality and Uniformity of Hydrothermally Grown ZnO Nanowires by Surface Activation of Catalyst Layer', *Nanoscale research letters*. SpringerOpen, 12(1), pp. 1–8.

Murillo, G., Rodríguez-Ruiz, I. and Esteve, J. (2016) 'Selective Area Growth of High-Quality ZnO Nanosheets Assisted by Patternable AlN Seed Layer for Wafer-Level Integration', *Crystal Growth & Design*, 16(9), pp. 5059–5066. doi: 10.1021/acs.cgd.6b00661.

Özgür, U. *et al.* (2005) 'A comprehensive review of ZnO materials and devices', *Journal of Applied Physics*, 98(4), p. 041301. doi: 10.1063/1.1992666.

Panda;, S. K. *et al.* (2013) 'Schottky nanocontact on single crystalline ZnO nanorodusing conductive atomic force microscopy', *Journal of Nanoparticles Research*, 15(12), p. 1361.

Riaz, M. *et al.* (2011) 'Study of the Piezoelectric Power Generation of ZnO Nanowire Arrays Grown by Different Methods', *Advanced Functional Materials*, 21(4), pp. 628–633. doi: 10.1002/adfm.201001203.

Stitz, N. *et al.* (2016) 'Piezoelectric Templates – New Views on Biomineralization and Biomimetics', *Scientific Reports*. The Author(s), 6, p. 26518. doi: 10.1038/srep26518https://www.nature.com/articles/srep26518#supplementary-information.

Su, T. (2017) 'Origin of surface potential in undoped zinc oxide films revealed by advanced scanning probe microscopy techniques', *RSC Advances*. The Royal Society of Chemistry, 7(67), pp. 42393–42397. doi: 10.1039/C7RA06117J.

Tamvakos, D. *et al.* (2015) 'Piezoelectric properties of template-free electrochemically grown ZnO nanorod arrays', *Applied Surface Science*, 356, pp. 1214–1220. doi: https://doi.org/10.1016/j.apsusc.2015.08.187.

Vayssieres, L. (2003) 'Growth of Arrayed Nanorods and Nanowires of ZnO from Aqueous Solutions', *Advanced Materials*, 15(5), pp. 464–466. doi: 10.1002/adma.200390108.

Wang, Z. L. (2009) 'ZnO nanowire and nanobelt platform for nanotechnology', *Materials Science and Engineering R: Reports*, 64(3–4), pp. 33–71. doi: 10.1016/j.mser.2009.02.001.

Wang, Z. L. *et al.* (2010) 'Lateral nanowire/nanobelt based nanogenerators, piezotronics and piezo-phototronics', *Materials Science and Engineering R: Reports*. Elsevier B.V., 70(3–6), pp. 320–329. doi: 10.1016/j.mser.2010.06.015.

Wang, Z. L. (2010) 'Piezotronic and piezophototronic effects', *Journal of Physical Chemistry Letters*, 1(9), pp. 1388–1393. doi: 10.1021/jz100330j.

Wang, Z. L. (2012) 'From nanogenerators to piezotronics—A decade-long study of ZnO nanostructures', *MRS Bulletin*, 37(09), pp. 814–827. doi: 10.1557/mrs.2012.186.

Wang, Z. L. and Song, J. H. (2006) 'Piezoelectric nanogenerators based on zinc oxide nanowire arrays.', *Science (New York, N.Y.)*, 312(5771), pp. 242–6. doi: 10.1126/science.1124005.

Wen, C. *et al.* (2019) 'In Situ Observation of Current Generation in ZnO Nanowire Based Nanogenerators Using a CAFM Integrated into an SEM', *ACS Applied Materials & Interfaces*. American Chemical Society, 11(17), pp. 15183–15188. doi: 10.1021/acsami.9b00447.

Xu, S. *et al.* (2010) 'Self-powered nanowire devices', *Nature Nanotechnology*, 5(5), pp. 366–373. doi: 10.1038/nnano.2010.46.

Yang, F. *et al.* (2019) 'The high-speed ultraviolet photodetector of ZnO nanowire Schottky barrier based on the triboelectric-nanogenerator-powered surface-ionic-gate', *Nano Energy*, 60,

pp. 680–688. doi: https://doi.org/10.1016/j.nanoen.2019.04.015.

Yang, P. *et al.* (2002) 'Controlled growth of ZnO nanowires and their optical properties', *Advanced Functional Materials*, 12(5), pp. 323–331. doi: 10.1002/1616-3028(20020517)12:5<323::AID-ADFM323>3.0.CO;2-G.

Yang, Y. *et al.* (2012) 'Pyroelectric nanogenerators for harvesting thermoelectric energy.', *Nano letters*, 12(6), pp. 2833–8. doi: 10.1021/nl3003039.

Zhong, B. and Wang, L. (2007) 'Nanopiezotronics **', pp. 889–892. doi: 10.1002/adma.200602918.